An experiment in high-frequency sediment acoustics: SAX99

E. I. Thorsos[1], K. L. Williams[1], D. R. Jackson[1], M. D. Richardson[2], K. B. Briggs[2], D. Tang[1]

[1] Applied Physics Laboratory, University of Washington, 1013 NE 40th St, Seattle, WA 98105, USA.
eit@apl.washington.edu, williams@apl.washington.edu, drj@apl.washington.edu, djtang@apl.washington.edu
[2] Marine Geosciences Division, Naval Research Laboratory, Stennis Space Center, MS 39529, USA.
mike.richardson@nrlssc.navy.mil, kevin.briggs@nrlssc.navy.mil

Abstract

A major high-frequency sediment acoustics experiment was conducted in shallow waters of the northeastern Gulf of Mexico. The experiment addressed high-frequency acoustic backscattering from the seafloor, acoustic penetration into the seafloor, and acoustic propagation within the seafloor. Extensive in situ measurements were made of the sediment geophysical properties and of the biological and hydrodynamic processes affecting the environment. An overview is given of the measurement program. Initial results from APL-UW acoustic measurements and modelling are then described.

1. Introduction

"SAX99" (for sediment acoustics experiment - 1999) was conducted in the fall of 1999 at a site 2 km offshore of the Florida Panhandle and involved investigators from many institutions [1, 2]. SAX99 was focused on measurements and modelling of high-frequency sediment acoustics and therefore required detailed environmental characterisation. Acoustic measurements included backscattering from the seafloor, penetration into the seafloor, and propagation within the seafloor at frequencies chiefly in the 10-300 kHz range [1]. Acoustic backscattering and penetration measurements were made both above and below the critical grazing angle, about 30° for the sand seafloor at the SAX99 site. In addition, investigations of acoustic detection of buried targets were made at grazing angles below the critical angle. Acoustic measurements were also conducted after modifications were made to the seafloor: divers changed the interface roughness and introduced multiple small scatterers or isolated larger targets. Extensive *in situ* measurements were made of the seafloor sediment geophysical properties and of the meteorological, oceanographic, and biological processes affecting the acoustic environment [2]. Our goal was to characterise the seafloor environment in sufficient detail to permit accurate modelling of the acoustic measurements.

The goals of this paper are twofold: first, to provide an overview of the entire SAX99 measurement program, and second, to give initial results from APL-UW (Applied Physics Laboratory, University of Washington) measurements and modelling, the latter based largely on NRL-SSC (Naval Research Laboratory, Stennis Space Center) environmental measurements. Separate papers in this conference [3-7] describe other initial results.

2. Overview of SAX99

At the SAX99 site near Fort Walton Beach, Florida (30°22.7'N, 86°38.7'W) the water depth is 18-19 m, and the upper metre of the seafloor is composed of medium quartz sand (grain diameter 0.25-0.50 mm). A seafloor ripple field was present with wavelengths from 50 to 70 cm. The ripple height varied with time, but was usually 3-6 cm (peak to peak). Shell fragment layers were encountered in some areas within the top 1 m, and whole and broken sand dollar tests were also observed, usually below 20 cm depth. Further discussion of the properties of the SAX99 site is given in [2]. Two ships, the research vessel (*R/V*) *Seward Johnson* and the *R/V Pelican*, were used to support most measurements in SAX99, which extended from 28 September to 14 November 1999.

A variety of acoustic and environmental measurements were made during SAX99, and even separation into these two categories requires clarification, since acoustical techniques were used in many of the environmental measurements. In our terminology "acoustic measurements" yield information on topics such as seafloor backscatter that we seek to understand in terms of environmental descriptions obtained separately. Measurements made using acoustical techniques for the purpose of characterising the environment are considered "environmental measurements."

2.1 Acoustic Measurements

Backscattering data were collected from five separate towers placed on the bottom and from an ROV deployed from the *R/V Seward Johnson*, which had been placed in a four-point moor. Frequencies spanned the range from 2 kHz to 3 MHz, but further analysis is required to determine if data at frequencies below 20 kHz will yield reliable backscattering strengths. Some initial results for backscattering from the naturally rough seafloor are given in Section 3.1 and in Briggs *et*

TG Leighton, GJ Heald, HD Griffiths, G Griffiths, (eds.), 'Acoustical Oceanography', Proc. Institute of Acoustics Vol. 23 Part 2, 2001.

al. [3]. Investigations of backscattering from regions of the seafloor with well-defined treatments (or manipulations) are described in Richardson *et al.* [4] and Williams *et al.* [5].

Measurements were also made of acoustic fields transmitted across the water-sediment interface using two separate buried arrays as receivers. The motivation for making these acoustic penetration measurements was to investigate penetration at subcritical grazing angles [8, 9], an important issue for buried object detection. Initial results are given in Section 3.2 and in Chotiros *et al.* [7].

Studies of acoustic propagation within the seafloor apply to both acoustic and environmental measurement categories, and it is difficult even to make that separation. During SAX99 Stoll, Bibee, and Buckingham all measured low frequency (of order 100 Hz) sound speed in surficial sands at the SAX99 site [2]. (Complete names and affiliations of all investigators mentioned can be found in reference [1] or [2].) In preliminary analyses each group obtained values in the neighbourhood of 1600 m/s, much lower than the values measured by NRL-SSC at 38-400 kHz, which were in the neighbourhood of 1740-1780 m/s [2]. Analysis of sediment properties from vibra cores (Dewitt) and chirp sonar profiles shows a uniform sand bed up to 5 m thick, which suggests that low and high frequency measurements were made in the same sediment type. Some indication of velocity dispersion is also seen in APL-UW sound speed data, mainly at the low end (10-50 kHz) of the measurement frequency range which extended from 10 kHz to 300 kHz. Initial analysis of the entire set of sound speed and attenuation data, using sediment geophysical properties measured at the SAX99 site, shows it to be generally consistent with that expected for the Biot model [10] of sound propagation in poroelastic media.

At frequencies above about 100 kHz, attenuation data obtained with an APL-UW diver-deployed attenuation array show substantial variability from path to path and from deployment to deployment. (In the 10-kHz to 50-kHz frequency range significant variability was not observed.) In some cases the attenuation varies ± 20 dB/m about the mean level, which suggests that scattering, perhaps from buried shells or other heterogeneities, is significantly affecting the propagating field at these higher frequencies. Thus, it is necessary to distinguish between the intrinsic attenuation and attenuation that includes the effects of scattering. This distinction is important because only the intrinsic attenuation should be compared directly with Biot model predictions.

Acoustic detection of buried targets involves the three main acoustic processes studied during SAX99: backscattering from the sediment, penetration into the sediment, and propagation within the sediment. Thus, several sets of buried target detection measurements were made during SAX99. In one, Christoff and Commander used a towed synthetic aperture sonar (SAS) system [11] to investigate target detections at the SAX99 site. They also made measurements in similar sediments at a site 87 km ESE near Panama City, where several cylindrical targets had been buried in April 1999 (before the final SAX99 site had been selected). A target buried 50 cm deep (to the top of the target) can be clearly seen in an SAS image obtained at the site near Panama City (Figure 1) showing that deeply buried targets can be detected acoustically at angles well below the critical angle. APL-UW results from acoustic penetration studies, described in Section 3.2, indicate that scattering from sediment ripples (roughness) is the dominant mechanism that couples energy into the sediment at subcritical grazing angles and thereby makes these subcritical target detections possible.

2.2 Environmental Measurements

The physical and biological measurements made during SAX99 are described in reference [2]. In general terms, the goals of the sediment geophysical measurements were to determine the mean values, vertical gradients, and spatial variability (to centimetre scales) of the sediment properties relevant to acoustic scattering from the seafloor. An important goal was to determine values for all of the parameters that enter into a Biot model description of the sediment [10]. Biological and hydrodynamic processes were examined in order to understand their effects on the spatial and temporal variability of the sediment properties and roughness, and the potential impact of these processes on high-frequency acoustics.

The physical properties of the sediment and water column were examined in detail. A Simrad EM 3000 multibeam echosounder obtained high-resolution bathymetry in the region of the site (Flood). Stereo-photographic images of the water-sediment interface were made to characterise the interface roughness (Briggs, Lyons, and Wheatcroft). Investigators from NRL-SSC (Richardson, Briggs, Lavoie, Reed, Bibee, and others) made extensive environmental measurements, largely *in situ*, needed to define Biot model parameters (these include compressional and shear wave speed and attenuation, conductivity, and sediment permeability). They used *in situ* resin impregnation for analysis of sediment microstructure, and collected sediment cores (for porosity, bulk density, grain density and bulk modulus, mean grain size, and percent gas in the sediment). They also conducted side scan sonar and drift camera surveys, and participated in numerous sediment manipulations to observe the effects of discrete scatterers or changing roughness on acoustic backscattering. A chirp sonar was used to study sediment subsurface structure in the vicinity of the measurement site (Schock). The rapid temporal changes in seafloor roughness were measured with a laser profiler (Jaffe and Moore). Sediment volume heterogeneity was examined with digital X-radiography, and high-resolution sediment porosity was obtained with a diver-deployed conductivity probe (Wheatcroft). An acoustic tomographic imaging system was used to measure sediment sound speed variability, and sediment porosity variability and seafloor roughness were examined with a sediment conductivity probe system (Tang). A high-precision resistivity array was also used to measure porosity variability (Jackson and Gunn). *In situ* permeability versus depth was measured (Johnson, Bennett). Cores were collected for later analysis of sediment microfabric (Bennett) and for later analysis of high-resolution density heterogeneity via X-

ray CT analysis (Orsi). A wave buoy was used to obtain surface wave spectra (Dahl). Other environmental properties (including wind speed and direction; profiles of water column sound speed, temperature and conductivity; tides; surface wave heights; and current speed and direction) were monitored with shipboard CTDs, meteorlogical instruments, and acoustic doppler current profilers (ADCP) and NRL-SSC bottom-mounted ADCPs and pressure and conductivity sensors.

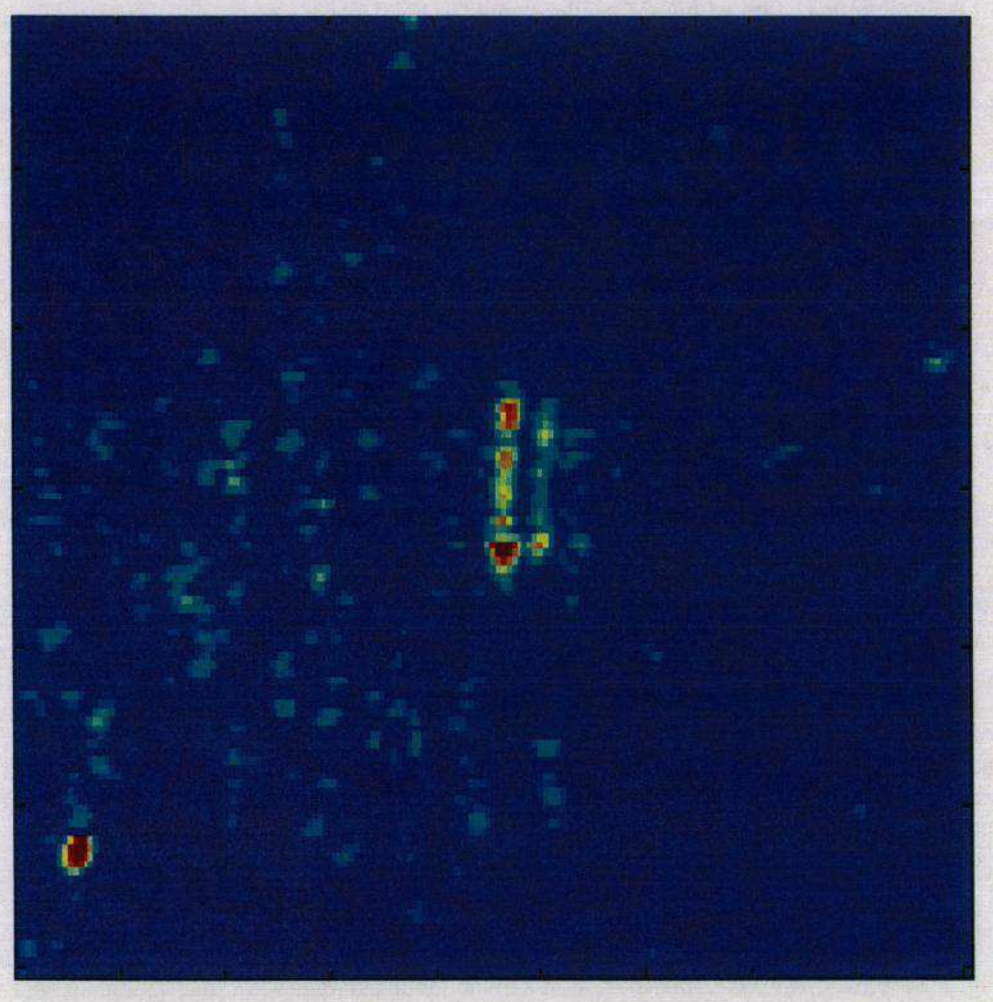

Figure 1. SAS image of a cylindrical target buried 50 cm deep. The field of view is about 9 m by 9 m, the buried target is near the centre, and the feature in the lower left corner is a marker on the sediment surface. The 20 kHz sound was incident from the left at a range of 50 m from the cylindrical target which had a length of 192 cm and a diameter of 47 cm. The range combined with the height of the towbody above the bottom (4.0 ± 0.5 m) leads to an incident grazing angle at the bottom of 4° to 5°, far below the critical angle of 30°. The peak target return is about 22 dB above background level, which is due to backscattering from the seafloor.

Effects of biological processes were studied both within the sediment and in the water column. Effects of defaunations and of concentrations of sand dollars on acoustic backscatter were examined in selected study areas (Jumars, Self, and Schmidt). A study was made of microbial abundance and its spatial distribution relative to sand grain contacts (Jumars and Schmidt). Emergence traps were deployed and monitored (Self, Thistle, and Suderman). Zooplankton and nekton migration were monitored through a lunar cycle using high-frequency acoustics (Holliday, Greenlaw, and McGehee). Sediment concentrations and benthic fluxes of methane and oxygen were measured during a site survey in July 1999 in order to bound the sediment bubble concentration (Martens and Albert).

Findings from the broad range of the environmental measurements made during SAX99 will be used in ongoing investigations to more fully understand qualitative aspects of acoustic processes and to provide inputs for quantitative modelling of acoustic measurements.

3. Initial APL-UW Results

The remainder of this paper is devoted to initial experimental and modelling results of the APL-UW group. The specific topics covered are acoustic backscattering and acoustic penetration at subcritical grazing angles; for the cases examined here the seafloor was not modified by divers. As mentioned previously, the acoustic modelling is based largely on sediment physical properties measured by NRL-SSC investigators.

3.1 Backscattering from natural sediment

The objectives for examining backscattering from natural sediments in SAX99 were to identify the dominant backscattering mechanisms and to demonstrate that the backscattered field can be quantitatively modelled based on measured sediment properties. Models for bottom backscattering generally account for scattering from bottom roughness and for scattering from sediment heterogeneity (i.e., sound speed and density variability) [12]. As discussed below, initial model results for the SAX99 site show sediment heterogeneity scattering to be negligible in comparison to sediment roughness scattering at 40 kHz. In addition, backscattering predictions based on rough surface perturbation theory are found (in unpublished work by Grochocinski, Williams, and Jackson) to differ by about 2 dB depending on the choice made for the sediment model (fluid or Biot). Thus, data/model comparisons for backscattering may also serve to demonstrate whether a sediment Biot model yields more accurate backscattering predictions than a sediment fluid model. However, to distinguish between these two models, it is necessary to pay unusually close attention to both measurement and modelling uncertainties.

Backscattering measurements were made with three systems: BAMS (40 kHz and 300 kHz), XBAMS (300 kHz), and STMS (20 to 150 kHz). BAMS (the Benthic Acoustic Measurement System) [13, 14] and XBAMS ("Xcelerated" Benthic Acoustic Measurement System), which is similar to BAMS, collected backscattering data autonomously from 75-m diameter circular areas over the duration of the experiment. However, the effective diameter was 36 m in order to avoid contaminating effects of sea surface scattering. The third acoustic system, the Sediment Transmission Measurement System (STMS), was newly constructed for SAX99 and used to carry out a variety of measurements under real-time user control. These included backscattering measurements at 20 to 150 kHz and penetration measurements at multiple grazing angles at 10 to 50 kHz. To obtain backscattering strengths, it is necessary to measure scattering from many independent areas on the bottom so that the average scattered intensity can be estimated. The STMS tower was repositioned repeatedly by divers to give the needed measurements from independent patches of the bottom. The sonars on the BAMS and XBAMS towers rotate in azimuth in steps of the horizontal beam widths, which are small (5° for BAMS at 40 kHz and 1° for BAMS and XBAMS at 300 kHz). Thus, ensemble averages of backscattered intensity needed for backscattering strengths could be obtained without diver intervention.

Bottom backscattering strengths at 40 kHz measured close in time with BAMS (asterisks) and STMS (circles) are shown in Figure 2. The STMS site was about 200 m east of the BAMS site, the STMS measurements were made on 26 October 1999, and the BAMS data are from 25-28 October. During this period three of the four quadrants around BAMS were being used for sediment treatment experiments, leaving only one quadrant for scattering from natural sediment. Thus, results over the natural sediment quadrant were used on four successive nights to obtain the equivalent of a full scan of independent samples. Scattering from fish was sometimes evident during the day (e.g., mid-day fluctuations over days 9-13 in Figure 1 in [4]), and this was avoided using BAMS data near midnight. STMS data were taken during the day, but coherent averaging over multiple pings was used to effectively eliminate effects of fish scattering. The error bars denote statistical uncertainty combined with estimates for systematic uncertainty. Scattered intensities for 20 and 72 independent bottom patches were averaged to obtain the scattering strengths from STMS and BAMS data, respectively. The statistical error is less for the BAMS data set, but the estimated systematic uncertainty is greater, and as a result the total uncertainty is nearly the same for the two systems.

The trends of the two data sets in Figure 2 appear to show an offset of about 2 dB, especially when viewed relative to the trends of the model curves (to be discussed shortly). A similar comparison [15] using the same STMS data but combined with BAMS results from a single complete scan on 6 October 1999 showed no apparent offset. This indicates that spatial and/or temporal variability of seafloor properties can lead to backscattering variability at the SAX99 site, which suggests added caution when making inferences from data-model comparisons.

Model predictions of backscattering strength can be made for scattering from sediment roughness and for scattering from sediment heterogeneity at centimetre scales if appropriate sediment characterisations have been made. There is no evidence to suggest that scattering from gas bubbles on or within the sediment was important during SAX99. Preliminary modelling of scattering from sediment heterogeneity based on parameters given in Table 2 of [3] produce backscattering levels well below those for seafloor roughness scattering (about 25 dB lower at angles below the critical angle, and about 17 dB lower above the critical angle). Thus, we consider only scattering from sediment roughness, and use perturbation theory to model the scattering [12]. The most important

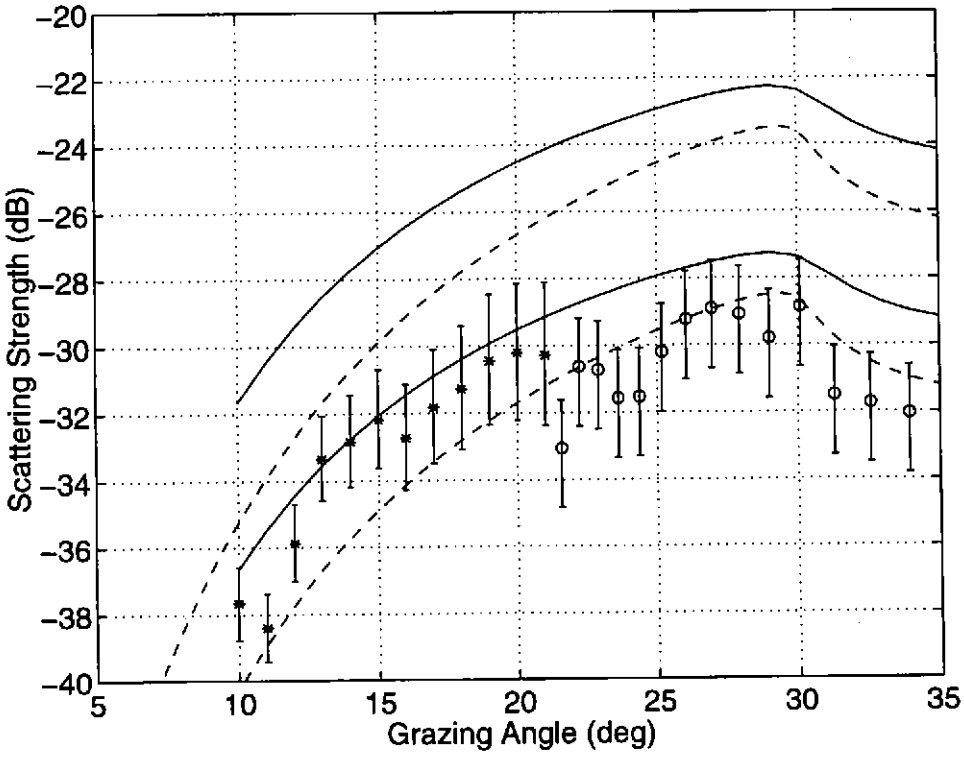

Figure 2. Bottom backscattering strengths at 40 kHz. The circles and asterisks denote results from STMS and BAMS, respectively. The two sets of curves are the uncertainty bounds for model results based on fluid (solid curves) and Biot (dashed curves) models for the sediment using roughness data measured near BAMS.

environmental descriptor is the spectral strength of roughness at the "Bragg wavenumber" $k_B = 2k\cos\theta_i$, where $k = 2\pi/\lambda$ is the acoustic wavenumber in water, λ is the acoustic wavelength in water, and θ_i is the incident grazing angle. Stereo photogrammetric roughness data for SAX99 are now becoming available [3] and provide estimates of 1-D roughness spectra. In addition, Tang's *in situ* conductivity probe data has been used to obtain 1-D roughness spectral estimates. This was possible because the sediment surface profile can be obtained from conductivity data signatures that accurately give the heights of the probes as they first enter the sediment. The array of 16 probes with 1-cm separation was precisely incremented in steps of 1.5 or 2.0 cm in the direction perpendicular to the array axis, which yielded measurements of the sediment surface profile.

The model curves in Figure 2 are based on stereo photogrammetric data measured at the BAMS tower site on 23 October and 5 November 1999 [3]; the spectral levels are nearly the same for these two dates in the region of the Bragg wavenumbers for backscatter. A power-law fit was made to the average 1-D spectrum for these dates over the spatial frequency ($1/\lambda$) range of 0.2 to 2.0 cm^{-1} which contains the relevant Bragg spatial frequencies (e.g., $k_B/(2\pi) = 0.505$ cm^{-1} at $\theta_i = 15°$). This gave $w_1 = 0.00114$ cm^3 and $\gamma_1 = 2.05$, where w_1 is the 1-D roughness spectral strength (or spectral intercept) and γ_1 is the spectral exponent (or negative of the spectral slope). On the assumption of isotropic roughness, the corresponding 2-D power-law parameters are found [16] to be $w_2 = 0.004$ cm^4 and $\gamma_2 = 3.05$. The statistical uncertainty for the spectral strength parameter is estimated [3] to be +2 dB to -3 dB (for 95% confidence) on the assumption of spatial stationarity of roughness. This uncertainty is taken into account in Figure 2, where only the upper and lower prediction bounds for the two sediment models are shown. The mean predictions are not shown, but would be 3 dB above the lower curves in each case.

The additional inputs required for the sediment fluid model are the sediment-water sound speed and density ratios (1.16 and 2.03, respectively), and the compressional wave attenuation (0.307 dB/m/kHz corresponding to a loss parameter [16] $\delta = 0.01$). The sound speed ratio results from a 1530 m/s water sound speed near the seafloor [2] and an average 1775 m/s sediment sound speed inferred from several APL-UW and NRL-SSC measurement systems at frequencies above 100 kHz. The attenuation and corresponding loss parameter were inferred from *in situ* measurements (10 to 50 kHz).

At this stage in our analysis the parameters required for the Biot sediment model have been obtained through a combination of direct measurements and optimisation of Biot model agreement with velocity dispersion and attenuation data. The results are as follows: porosity (0.38), grain density (2690 kg/m^3), fluid density (1023

kg/m^3), grain bulk modulus (2.5×10^{10} Pa), frame modulus ($(4.36 - 0.208i) \times 10^7$ Pa), frame shear modulus ($(1.98 - 0.1188i) \times 10^7$ Pa), water bulk modulus (2.3947×10^9 Pa), viscosity (0.001 kg/m· s), permeability (4.0×10^{-11} m^2), and tortuosity (1.2). The pore size parameter $a_p = 2.25 \times 10^{-5}$ m is found [17] from $a_p^2 = 4t\kappa/\beta$, with t the tortuosity, κ the permeability, and β the porosity. One unsettling aspect of this optimisation procedure is that the Biot parameters do not reproduce the exact parameters used in the fluid sediment model, though the sound speed and density ratios are quite close. The sediment compressional wave speed in the Biot model is 1775 m/s at 150 kHz, and this reduces to 1770 m/s at 40 kHz which gives a sound speed ratio of 1.157. The density ratio is 2.01, close to the fluid model value of 2.03. However, the attenuation at 40 kHz is only 0.183 dB/m/kHz, about 60% of the fluid model value. When these Biot values for sound speed and density ratios and attenuation are used in the fluid model, the scattering level is increased by a maximum of 0.3 dB below the critical angle, and decreased a maximum of 0.3 dB above the critical angle. Thus, the differences in these common parameters between the two models are not responsible for the differences in scattering strength predictions.

Note that in Figure 2 the Biot model results lie about 2 dB below those for the fluid model, and that the model uncertainty is significant. Note also that the dip in backscattering strength for grazing angles above 30° occurs for the model curves and experimental results. This effect in the model curves results from the 30° critical angle, since above the critical angle more energy is transmitted into the sediment, and this leads to less backscattering from the rough interface. The similar dip in the measured scattering strengths supports sediment roughness scattering as being the most important backscattering mechanism at grazing angles near 30° and frequencies near 40 kHz for the sandy sediments at the SAX99 site.

The roughness spectrum used for the model curves in Figure 2 was obtained near BAMS from measurements that bracket the time period of the BAMS acoustic data. For the BAMS data alone, the data-model comparison appears to be better for the Biot sediment model than for the fluid sediment model. However, considering both the data and model uncertainties, it is not possible to rule out the fluid sediment model at this time based on backscatter data alone. Briggs [3] obtained stereo photogrammetric roughness data on 4 November at the APL-UW penetration site, which is close to the site of STMS backscatter measurements. The spectral levels were found to be higher than at the BAMS site. However, fish were observed to congregate near the equipment at the penetration site, and to cause increased small-scale bottom roughness as a result of their feeding activity. This activity did not extend to the region of nearby backscattering measurements, and thus we do not believe the roughness levels measured at the penetration site should apply to STMS backscatter measurements.

The offset in backscattering strength measurements by BAMS and STMS during a similar time period raises questions about system accuracy and spatial stationarity of roughness. We believe the system uncertainty is about 1 dB for both BAMS and STMS (slightly higher for BAMS); thus, limitations in system accuracy cannot be ruled out as the cause of the offset.

We have been able to gain some insight on the degree of spatial variability in spectral estimates using data from Tang's conductivity probe system. From measurements on 17 October 160 m south of STMS, on 18 October 240 m north-northwest of STMS, and on 24 October 160 m east of STMS, 1-D power-law spectra were obtained with spectral strengths at the appropriate Bragg wavenumbers that ranged from about 4 dB above to about 4 dB below the average spectrum for 23 October and 5 November data obtained by Briggs with stereo photogrammetry [3]. It would appear superficially that this magnitude of variation would indicate non-stationarity in space and possibly in time, but a detailed statistical analysis would be required to be certain. In any case, it is at least plausible that the differences in the trends in the BAMS and STMS scattering strengths shown in Figure 2 could be due to different roughness conditions at the two sites. It also seems clear that in order to reduce model uncertainties sufficiently to permit an unambiguous test of fluid and Biot sediment models for backscatter, the sediment roughness would need to be measured over a larger area in the region of the backscatter measurements than is presently done.

3.2 Acoustic penetration in natural sediment

The objectives for examining acoustic penetration into natural sediments were to identify the dominant penetration mechanisms, and to demonstrate that the penetrating field can be quantitatively modelled based on measured sediment properties.

The diver-movable STMS source tower could be repositioned to change the incident grazing and azimuthal angles. The penetrating fields were measured with an array of 30 buried hydrophones composed of 5 vertical arrays of 6 hydrophones each [1]. The hydrophones were inserted into position by divers using rods that were extended horizontally from a nearby cofferdam that had been sunk into the sediment and then excavated. The rods were then removed leaving the hydrophones in place without disturbing the sediment surface. The top hydrophone in each vertical array was no closer than 5 cm from the sediment surface, and the bottom hydrophone was at a depth of about 45 cm. After insertion the hydrophone positions were accurately determined (within 0.5 cm) with acoustic surveying techniques and subsequent optimisation.

Transmission data from the tower to the buried array were taken at 8 centre frequencies from 10 to 50 kHz. For each source and centre frequency, several transmissions (normally less than 10, but in some cases up to 100) were sent so that coherent averaging could be used to reduce the effect of schools of fish sometimes present in the field of view. Penetration data from the buried array has been used to produce speed-angle plots [9] for the penetrating field, and these have been compared with the corresponding plots produced by simulations. Perturbation theory has been used to account for scattering at the sediment surface in these simulations [9], and preliminary models have been used for ripple field roughness and for small-scale roughness based on the available information discussed further below. When the incident angle is above the critical angle, the dominant penetrating field is due to refraction, and data/simulation speed-angle plots are in very good agreement [15]. For these above-critical-angle cases, simulation results are insensitive even to the large-scale ripple, and measurements with diver-smoothed sediments or simulations with a flat surface are essentially identical.

The results of penetration measurements with the incident grazing angle below the critical angle are shown on the left side of Figure 3. While the sediment sound speed is known, both real and simulated data (panels on right side in Figure 3) are processed [9] as if the sound speed were unknown.

In order to simulate the measured speed-angle plots in Figure 3, it is highly desirable to use a deterministic model for the large-scale ripple field, but this was not directly measured during SAX99. Thus a deterministic 1-D ripple field model was estimated based on ripple wavelength (48 cm) and height (1 cm rms) determinations from conductivity probe data, and ripple phase and azimuth from diver video taken at the site of the buried array. In this case the STMS source tower was positioned such that the propagation direction of the incident field above the buried array was only about 15° off in azimuth from being perpendicular to the ripple crests. Small-scale, isotropic roughness was also included using power-law roughness parameters $w_2 = 0.004$ cm^4 and $\gamma_2 = 3.0$. We find that small-scale roughness plays almost no role in simulations of speed-angle plots when large-scale ripple is present.

A fluid model was used for the sediment in our penetration simulations. The required model parameters are the water and sediment sound speeds (1530 m/s and 1775 m/s, respectively), the density ratio (2.0), and the compressional wave attenuation, which is given as a function of frequency by the loss parameter [16] $\delta = 0.01$. The normalisation procedure used with the buried hydrophone signals [9] eliminates sensitivity to the sediment absorption coefficient. The transmitted waveform had a smooth bell-shaped envelope which was approximated by the Gaussian $\exp(-t^2/t_s^2)$ with $t_s = 65$ μs for 20 kHz and with $t_s = 50$ μs for 30, 40, and 50 kHz.

We consider the agreement between the measured and simulated speed-angle plots to be very good, given that the ripple profile is not precisely known. In particular, while 2-D surface realisations are used in the simulations, we have used a simple sine wave for the ripple in these simulations. For the simulated speed-angle ambiguity plots, it is known with certainty that the sediment sound speed is 1775 m/s, and there are no propagating waves at other speeds. Thus, the complex structure in the simulated ambiguity plots is a result of propagating energy at 1775 m/s (giving the main lobe, which is the right-most red feature in the upper three panels on the right), a small set of strong sidelobes distributed along a line which extends from the main lobe toward zero speed and zero depression angle, and a large number of weak sidelobes distributed over the entire space of the plot. The relatively strong sidelobes are a result of the sparseness of the buried array. Indeed, if a simulated 20 kHz plane wave pulse propagates through the array at a 25° depression angle, the response is very close to that in the upper right-hand panel. While the simulations at 20, 30, and 40 kHz each show a relatively strong feature on the Snell's law curve, it is obvious these are sidelobes, and there is no propagating energy that obeys Snell's law. Clearly, in the simulations, no significant energy is reaching the buried array via refracted paths; instead, scattering from the sediment roughness is responsible for the penetration. We believe the excellent correspondence between measured and simulated speed-angle plots indicates that the same interpretation carries over to the measurements as well. Simulations without large-scale ripples lead to much less penetration and poor correspondence between measured and simulated speed-angle plots. Thus, scattering from the large-scale ripple field is quite clearly the dominant subcritical penetration mechanism for our measurements during SAX99. (The importance of the large-scale ripple to subcritical penetration has also been emphasised in other recent work [18,19].) Although it has been suggested that a Biot slow wave might be observed in this environment [8], our results to date give no indication of propagating waves in the sediment with wave speeds smaller than the expected compressional wave speed.

The frequency dependence of the speed-angle plots in Figure 3 is similar for measured data and simulations. At 20 kHz the main lobe of propagating energy for the measured data has a depression angle of about 20°, and at 30 and 40 kHz the depression angle steadily diminishes. At 50 kHz, a dominant propagating lobe is not even present. Simulations show the same behaviour, except the depression angle of the main lobe is slightly greater at the first three frequencies. This reduction in depression angle as the frequency increases, and the existence of a "frequency cut-off" between 40 and 50 kHz can be readily understood as an effect of scattering from quasi-periodic roughness. For simplicity, suppose we consider the sediment ripple to be represented by a monochromatic sine wave of wavelength 48 cm (as assumed in the simulations), and also take the direction of the incident wave to be perpendicular to the ripple crests. Attenuation will also

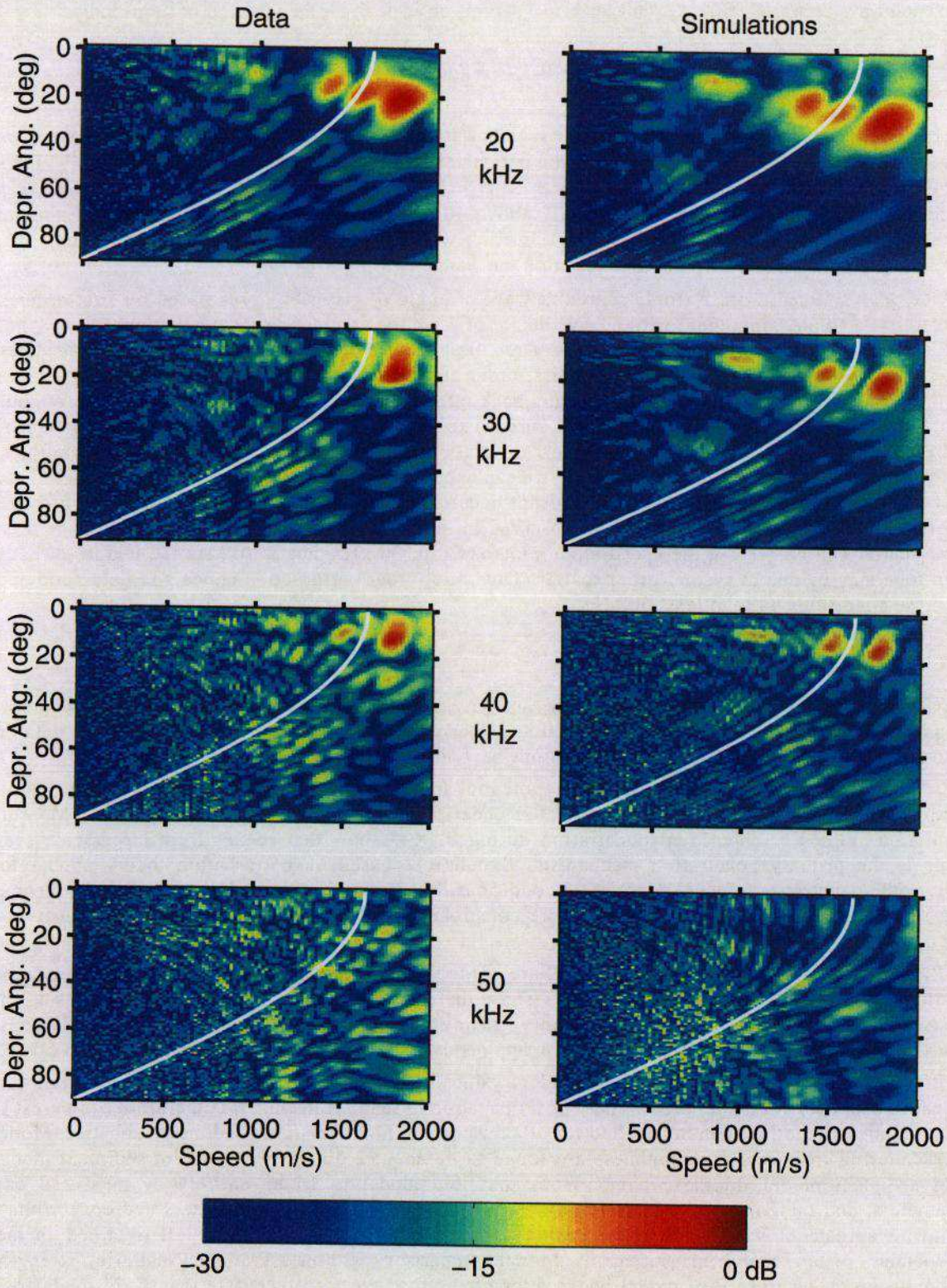

Figure 3. Measured (left) and simulated (right) speed-angle plots for acoustic penetration into sandy sediment with an incident grazing angle of 21.4°, well below the critical angle of 30°. The white line shows speed-angle combinations consistent with Snell's law of refraction.

be ignored for simplicity. Then regarding penetration, the effect of the ripple with wave vector $\boldsymbol{K}_r$ in a perturbation analysis is to scatter an incident plane wave in the water with horizontal wave vector $\boldsymbol{K}_i$ into a transmitted plane wave with horizontal wave vector $\boldsymbol{K}_2 = \boldsymbol{K}_i - \boldsymbol{K}_r$. This leads to a depression angle θ_2 for the scattered wave given by

$$\cos\theta_2 = \frac{c_2}{c_1}\left[\cos\theta_i - \frac{\lambda_1}{\lambda_r}\right] \tag{1}$$

where c_2/c_1 is the sound speed ratio, θ_i is the incident grazing angle, λ_1 is the acoustic wavelength in water, and λ_r is the ripple wavelength. Using the simulation parameters, one finds $\theta_2 = 26.5°$ for 20 kHz, 16.9° for 30 kHz, and 9.0° for 40 kHz. At 50 kHz (1) gives $\cos\theta_2 > 1$; in other words, the first-order scattered wave has become evanescent leading to the observed "cut-off" above 40 kHz. The trends in both the data and simulations are in remarkably good agreement with this simple model, which further strengthens the finding that scattering from large-scale ripple was the dominant penetration mechanism during SAX99

The analysis leading to a ripple-scattered wave at angle θ_2 given by (1) is based on first-order perturbation theory. For a ripple component with an rms height of 1 cm (as assumed in the simulations), $k_1 h = 0.82$ at 20 kHz and is even higher at the higher frequencies. Thus, first-order perturbation theory might be considered suspect in this context. However, as discussed in [9], first-order perturbation theory remains accurate to higher values of $k_1 h$ for the penetration problem than for scattering back into the water. For the case of scattering from quasi-periodic ripple, the speed-angle plots illustrate this accuracy explicitly. Lowest-order perturbation theory leads to a lobe of scattered energy at a well-defined depression angle as seen in Figure 3. When the next order in the small height perturbation expansion becomes significant, we can expect to see noticeable energy being scattered at about twice the fundamental depression angle. This will not occur in the present simulations (since they are based on first-order perturbation theory), but would be observed in the data if significant. No strong evidence of such higher-order scatter can be seen in the speed-angle plots at 20 or 30 kHz, but at 40 kHz the feature directly below the main lobe may be due to second-order scatter. Thus, first-order perturbation appears to be a good approximation for these conditions up to at least 30 kHz.

4. Concluding Remarks

SAX99 has provided a wealth of acoustic and environmental data in the area of high-frequency sediment acoustics, and our analysis of the data is still at an early stage. The breadth and quality of the data have allowed us to address a number of fundamental questions beyond the scope of previous investigations.

SAS images of buried targets show the potential for high-frequency buried target detections at subcritical grazing angles, and illustrate the need to better understand the acoustic penetration process. Measurements and simulation studies of subcritical penetration during SAX99 show that scatter from large-scale seafloor ripple fields is the primary penetration mechanism. Simulations based on perturbation theory appear to accurately capture the penetration process for SAX99 conditions, but for greater ripple heights or for frequencies above 30 kHz it may be necessary to use methods more comprehensive than first-order perturbation theory in simulations and models.

Backscatter data collected during SAX99 are of high quality, and the grazing angle dependence clearly shows predicted critical angle effects. The results show that scattering from small-scale roughness is the dominant backscattering mechanism at low-to-moderate grazing angles and at frequencies near 40 kHz. Other SAX99 results not reported here show this conclusion applies over the range from 20 kHz up to at least 50 kHz.

Preliminary analysis of frequency dependent values of sound speed and attenuation measured during SAX99 appear to support Biot model predictions for propagation in sand sediments. It is therefore of interest to determine if Biot model predictions can be verified for other aspects of high-frequency sediment acoustics. Model results for backscattering from seafloor roughness are found to be about 2 dB lower for a Biot sediment model than for a fluid sediment model. In these comparisons the fluid model is driven entirely by measured environmental parameters, and the Biot model is driven by a combination of measured parameters and constraints imposed by requiring agreement with velocity dispersion and attenuation data, which are all obtained in measurements independent of backscatter measurements. Model comparisons with measured backscattering strengths are as yet inconclusive on whether Biot model backscatter predictions are more accurate than fluid model results. A key difficulty for such an analysis is the need to obtain an accurate estimate of the average seafloor roughness spectrum over the entire region of the backscatter measurements, a measurement not yet attempted in any experiment. It may be necessary to address this question in future experimental work.

The relative accuracy of Biot and fluid sediment models also arises as an issue for simulation and modelling of subcritical penetration. For the speed-angle plots discussed in this paper, the magnitude of the penetrating field plays a minor role, and thus for these measures of penetration we would expect little sensitivity to the sediment model choice for the normal (fast) compressional wave. However, the magnitude of the penetrating field would be

important in the context of buried target detection, and thus the question of Biot versus fluid for penetration analysis also needs to be addressed.

At this stage of our analysis, the ability of the Biot model to capture the velocity dispersion and attenuation behavior and predict backscatter makes it our model of choice.

The work was supported by the U.S. Office of Naval Research and Naval Research Laboratory Program Element 061153N.

References

[1] Thorsos EI, Williams KL, Chotiros NP, Christoff JT, Commander KW, Greenlaw CF, Holliday DV, Jackson DR, Lopes JL, McGehee DE, Richardson MD, Piper JE and Tang D. An overview of SAX99: Acoustic measurements. *IEEE Journal of Oceanic Engineering*, in press.

[2] Richardson MD, Briggs KB, Bibee LD, Jumars PA, Sawyer WB, Albert DB, Bennett RH, Berger TK, Buckingham MJ, Chotiros NP, Dahl PH, Dewitt NT, Fleischer P, Flood R, Greenlaw CF, Holliday DV, Hulbert MH, Hutnak MP, Jackson PD, Jaffe JS, Johnson HP, Lavoie DL, Lyons AP, Martens CS, McGehee DE, Moore KD, Orsi TH, Piper JN, Ray RI, Reed AH, Self RFL, Schmidt JL, Schock SG, Simonet F, Stoll RD, Tang D, Thistle DE, Thorsos EI, Walter DJ and Wheatcroft RA. An overview of SAX99: Environmental considerations. *IEEE Journal of Oceanic Engineering*, in press.

[3] Briggs KB, Williams KL, Richardson MD and Jackson DR. Effects of changing roughness on acoustic scattering: (1) Natural changes, in *'Acoustical Oceanography', Proceedings of the Institute of Acoustics Vol. 23 Part 2, 2001*, T G Leighton, G J Heald , H Griffiths and G Griffiths, (eds.), Institute of Acoustics, (this volume), pp. 375-382.

[4] Richardson MD, Briggs KB, Williams KL, Lyons AP and Jackson DR. Effects of changing roughness on acoustic scattering: (2) Anthropogenic changes, in *'Acoustical Oceanography', Proceedings of the Institute of Acoustics Vol. 23 Part 2, 2001*, T G Leighton, G J Heald , H Griffiths and G Griffiths, (eds.), Institute of Acoustics, (this volume), pp. 383-390.

[5] Williams KL, Richardson MD, Briggs KB and Jackson DR. Scattering of high-frequency acoustic energy from discrete scatterers on the seafloor: Glass spheres and shells, in *'Acoustical Oceanography', Proceedings of the Institute of Acoustics Vol. 23 Part 2, 2001*, T G Leighton, G J Heald , H Griffiths and G Griffiths, (eds.), Institute of Acoustics, (this volume), pp. 369-374.

[6] Jackson DR and Richardson MD. Seasonal temperature gradients within a sandy seafloor: Implications for acoustic propagation and scattering, in *'Acoustical Oceanography', Proceedings of the Institute of Acoustics Vol. 23 Part 2, 2001*, T G Leighton, G J Heald , H Griffiths and G Griffiths, (eds.), Institute of Acoustics, (this volume), pp.361-368.

[7] Chotiros NP, Smith DE, Piper JN, McCurley BK, Lent K, Crow N, Banks R and Ma H. Acoustic penetration of a sandy sediment, in *'Acoustical Oceanography', Proceedings of the Institute of Acoustics Vol. 23 Part 2, 2001*, T G Leighton, G J Heald , H Griffiths and G Griffiths, (eds.), Institute of Acoustics, (this volume), pp. 355-360.

[8] Chotiros NP. Biot model of sound propagation in water-saturated sand. *Journal of the Acoustical Society of America* 1995; **97**: 199-214

[9] Thorsos EI, Jackson DR and Williams KL. Modeling of subcritical penetration into sediments due to interface roughness. *Journal of the Acoustical Society of America* 2000; **107**: 263-277

[10] Stoll RD. Sediment Acoustics. Volume 26 in Lecture Notes in Earth Sciences, edited by S. Bhattacharji *et al.* Springer-Verlag, Berlin, 1989, chapters 1 and 2

[11] Cutrona LJ. Comparison of sonar system performance achievable using synthetic-aperture techniques with nonsynthetic-aperture sonar systems. *Journal of the Acoustical Society of America* 1975; **58**: 336-348

[12] Williams KL and Jackson DR. Bistatic bottom scattering: Model, experiments, and model/data comparison. *Journal of the Acoustical Society of America* 1998; **103**: 169-181

[13] Dworski JG and Jackson DR. Spatial and temporal variation of acoustic backscatter in the STRESS experiment. *Continental Shelf Research* 1994; **14**: 1221-1237

[14] Jackson DR, Williams KL and Briggs KB. High-frequency acoustic observations of benthic spatial and temporal variability. *Geo-Marine Letters* 1996; **16**: 212-218

[15] Thorsos EI, Williams KL, Jackson DR and Tang D. High-frequency sound interaction in ocean sediments, in

Proceedings of the Fifth European Conference on Underwater Acoustics, ECUA 2000. Edited by Chevret P and Zakharia ME, Lyon, France, 2000.

[16] Jackson DR, Briggs KB, Williams KL and Richardson MD. Tests of models for high-frequency seafloor backscatter. *IEEE Journal of Oceanic Engineering* 1996; **21**: 458-470

[17] Johnson DL, Koplik J and Dashen R. Theory of dynamic permeability and tortuosity in fluid-saturated porous media. *Journal of Fluid Mechanics* 1987; **176**: 379-402

[18] Schmidt H and Lee J. Physics of 3-D scattering from rippled seabeds and buried targets in shallow water. *Journal of the Acoustical Society of America* 1999; **105**: 1605-1617

[19] Maguer A, Fox WLF, Schmidt H, Pouliquen E and Bovio E. Mechanisms for subcritical penetration into a sandy bottom: Experimental and modeling results. *Journal of the Acoustical Society of America* 2000; **107**: 1215-1225